Journal of
Synchrotron
Radiation

ISSN 0909-0495

Received 13 December 2011
Accepted 15 February 2012

Spectroelectrochemical cell for *in situ* studies of solid oxide fuel cells

Anke Hagen,* Marie Lund Traulsen, Wolff-Ragnar Kiebach and Bjoern Sejr Johansen

Department of Energy Conversion and Storage, DTU, Risoe Campus, Frederiksborgvej 399, Roskilde 4000, Denmark. E-mail: anke@dtu.dk

Solid oxide fuel cells (SOFCs) are able to produce electricity and heat from hydrogen- or carbon-containing fuels with high efficiencies and are considered important cornerstones for future sustainable energy systems. Performance, activation and degradation processes are crucial parameters to control before the technology can achieve breakthrough. They have been widely studied, predominately by electrochemical testing with subsequent micro-structural analysis. In order to be able to develop better SOFCs, it is important to understand how the measured electrochemical performance depends on materials and structural properties, preferably at the atomic level. A characterization of these properties under operation is desired. As SOFCs operate at temperatures around 1073 K, this is a challenge. A spectro-electrochemical cell was designed that is able to study SOFCs at operating temperatures and in the presence of relevant gases. Simultaneous spectroscopic and electrochemical evaluation by using X-ray absorption spectroscopy and electrochemical impedance spectroscopy is possible.

Keywords: XANES; *in situ*; SOFC; LSCF; impedance spectroscopy.

1. Introduction

Solid oxide fuel cells (SOFCs) produce electricity and heat from hydrogen- or carbon-containing fuels with high efficiencies and low pollution degrees; no NO_x or particles are emitted. CO_2, formed when using carbon-containing fuels, emerges concentrated and is thus cheaper to collect and to process further. SOFCs consist of two electrodes on the opposite sides of a solid electrolyte layer. The catalytic processes in a SOFC involve reduction of oxygen at the cathode, transport of oxygen ions through the cathode and electrolyte into the anode, where oxidation of the fuel (hydrogen, methane, carbon monoxide) occurs. Materials for state-of-the-art SOFCs comprise Ni/YSZ (yttria stabilized zirconia) anodes, YSZ electrolytes and LSM/YSZ (lanthanum strontium manganite) or LSCF (lanthanum strontium cobaltite ferrite) cathodes. Typical operating temperatures are in the range between 923 K and 1123 K (see, for example, Huang & Goodenough, 2009). One of the main challenges to be solved for SOFC technology is maintaining high performance over a long lifetime.

Large efforts have been focused on studying degradation processes, identifying origins of degradation and developing improved, more durable SOFCs [see recent status in the review by Knibbe *et al.* (2011)]. Usually, SOFCs are tested for electrochemical performance and afterwards (*post mortem*) structural and spectroscopic analysis is carried out. One of the problems with this approach is the lack of information under operating conditions, and the obtained results from *post mortem* evaluation are not always related to the actual performance/changes of performance. For detailed mechanistic studies on the microscopic/atomic level, materials, single crystals or specifically designed model systems are used instead of the full electrochemical cell, mostly owing to restrictions of the applied characterization method. *In situ* techniques have been developed to overcome this barrier.

The *in situ* studies investigated, for example, spectroscopic and structural properties separately from the electrochemical characteristics, often using model systems, *i.e.* material powders, instead of real electrochemical cells. The effect of oxygen partial pressure on barium strontium cobaltite ferrite perovskite-type SOFC cathode materials was, for example, investigated by Mueller *et al.* (2009) using XANES (X-ray absorption near-edge spectroscopy) and EXAFS (extended X-ray absorption fine structure) at relevant operating temperatures of 773–923 K, revealing the detailed reduction processes of the transition metals.

The recent progress of *in situ* investigations of SOFCs achieved by optical methods has been summarized by Pomfret *et al.* (2010).

Also, for other electrochemical devices, *in situ* methods have been further developed. The redox behaviour of cuprate- and nickelate-based electrodes for the direct electrochemical NO_x reduction was studied using *in situ* XANES at high

temperature and in the presence of relevant gases (NO or air) (Mueller *et al.*, 2009; Simonsen *et al.*, 2009). The results were related to separately determined electro-catalytic properties and the necessity of a combination of the two method approaches was concluded in order to be able to identify the relevant mechanisms.

The combination of an electrochemical cell with X-ray characterization was, for example, reported by Rodriguez *et al.* (2000), who successfully investigated Li-ion batteries. These *in situ* studies were carried out at room temperature. Also, for the study of Li-ion battery electrodes, an electrochemical *in situ* reaction cell was designed and successfully realised by Braun *et al.* (2003), allowing for the combination of XRD, ASAXS, XANES and EXAFS characterization.

Ultimately, it is desired to carry out studies under high-temperature conditions, where electrochemical cells like the SOFCs are operating, in order to understand phenomena which only occur under real operating conditions, *i.e.* under polarization (current/voltage). It is, for example, well known that some processes such as the activation of LSM-based cathodes in SOFCs are only occurring under polarization, which is therefore needed to elucidate the underlying mechanisms. Yildiz *et al.* (2006) investigated this effect on LSM and LSCM (lanthanum strontium calcium manganite) based electrodes deposited on single-crystal YSZ electrolytes and related the activation under polarization at higher temperatures to the change of the chemical state of lanthanum. Backhaus-Ricoult *et al.* (2008), on the other hand, studied the same subject on patterned LSM cathodes on YSZ electrolytes with an *in situ* photoelectron microscopy cell and suggested an extension of the active area for oxygen incorporation over the electrolyte surface by partially reduced manganese oxide species to be responsible for the activation. The mechanism of electrochemical oxygen reduction on samarium strontium cobaltite cathodes was studied in detail using *in situ* potential-dependent FTIR emission spectroscopy (Lu *et al.*, 2002).

These examples demonstrate that different spectroscopic methods can be applied during electrochemical operation of SOFCs. It is important though to consider the used SOFC configurations and sets of operating conditions before general conclusions can be drawn. For example, can the different studies reveal phenomena related to the surface, the bulk or interface and thus possibly give different feedback for the same system.

In this paper, an *in situ* cell is presented that enables the study of real electrochemical cells such as SOFCs at relevant temperatures and in the presence of relevant gases with respect to electrochemical and spectroscopic properties, using electrochemical impedance spectroscopy (EIS) and XANES, respectively.

A combination of these two methods was chosen as EIS is a powerful method for evaluating the resistances of the SOFC in detail; in particular, it is possible to deconvolute the total resistance of the SOFC into contributions from the single layers and processes in the cell (*e.g.* Højgaard Jensen *et al.*, 2009). The chemical and, to a lesser extent, electronic properties of the constituents of the SOFC can be characterized by using XANES, and the method can be carried out under conditions relevant for the electrochemical cells. In this paper the spectroelectrochemical cell was used for SOFCs. They were characterized by EIS and XANES under conditions typical for operation of a SOFC.

2. Experimental section

2.1. Samples

In order to verify the potential of the spectro-electrochemical cell, the following solid oxide cell configuration was chosen: on one side of the fuel cell a thin-film LSCF electrode ($La_{0.58}Sr_{0.4}Co_{0.2}Fe_{0.8}O_{3-\delta}$) was deposited by pulsed laser deposition onto a 500 µm-thick YSZ single crystal at 973 K and an oxygen partial pressure (pO_2) of 300 mtorr. The thickness of the electrode was ∼270 nm; on the other side of the electrolyte, the electrode was a ∼20 µm-thick conventional LSCF–CGO10 (cerium gadolinium oxide) composite electrode deposited by screen-printing on the YSZ single crystal. The cell was subsequently sintered at 1073 K for 72 h.

The cells were cut into 5 mm × 5 mm pieces. Pt-paste current collection layers were painted on the electrodes while leaving a small 1 mm × 1 mm area in the middle of the electrode free on the thin-film electrode that was used as the working electrode (see Fig. 1*a*). This area was used for detection of the fluorescence signal when recording the XANES spectrum. The cell was placed on the sample holder (see Fig. 1*b*) and heated to a temperature of 973 K in order to firmly attach the Pt onto the electrodes.

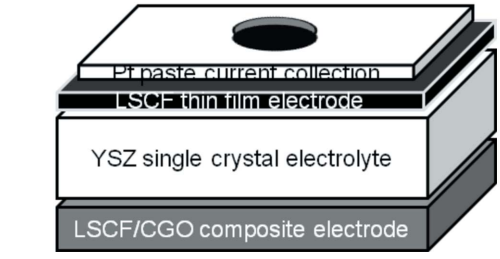

(*a*)

(*b*)

Figure 1
(*a*) Illustration of the fuel cell configuration: one thin film and one porous electrode on either side of a single-crystal electrolyte, Pt-paste current collection layer on top of the thin-film electrode. (*b*) Image of a 5 mm × 5 mm SOFC piece (grey) in the ceramic sample holder. Au wires are attached using the Pt current-collector layer (white); the spot in the centre marks the synchrotron beam inlet and fluorescence detection signal outlet.

To verify the results from the spectroelectrochemical cell, LSCF powders with compositions $La_{0.3}Sr_{0.7}Co_{0.5}Fe_{0.5}O_{3-\delta}$ (powder 1) and $(La_{0.6}Sr_{0.4})_{0.99}Fe_{0.8}Co_{0.2}O_3$ (powder 2) were investigated in another XANES cell set-up. About 3 mg of the powdered samples were mixed with ~20 mg alumina in a mortar, subsequently pressed to pellets of diameter 13 mm, and placed vertically in a glass *in situ* XANES cell heated by a tube furnace (for details, see Hagen, 2011). Here, spectra of the sample and the respective metal foil as reference were measured simultaneously in transmission.

2.2. Spectroelectrochemical cell

The cell (see Fig. 2) was made of aluminium with Kapton windows (~15 mm diameter) for the beam inlets and outlets straight through the cell and one larger 50 mm window perpendicular to the beamline for fluorescence detection. It is equipped with gas inlet and outlet fittings and an insert for the sample holder, including wires. Radiative heating was realised by an Osram lamp, and the sample was mounted 6 mm from the focal point of the Osram lamp, to avoid a too violent heating of the sample. The surroundings of the sample and the cell itself remained cold. Using this approach, active cooling to avoid high temperatures in the close vicinity of the spectroelectrochemical cell and at beamline components was not needed. If a voltage of 15 V is applied on the lamp, a black body in the focal point of the Osram lamp will be at 1573 K.

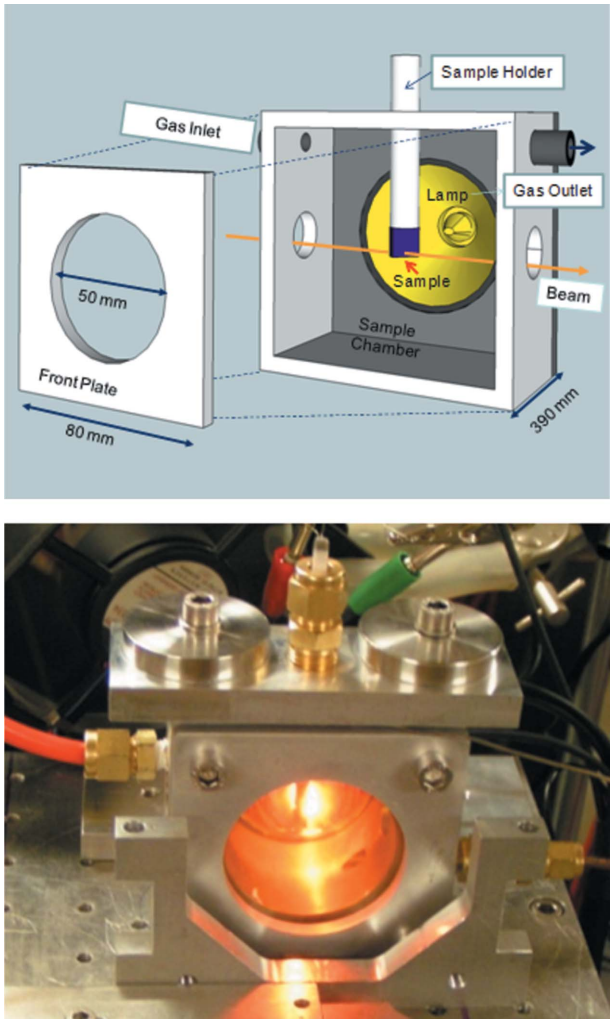

Figure 2
Drawing of the spectroelectrochemical cell and a photograph of it in operation. The sample holder is inserted vertically from the top. The heating lamp is on the back and a Kapton window, to measure the fluorescence, is in front of the cell.

The temperature was determined directly on the sample spot by combining EIS with knowledge of the conductivity of the YSZ electrolyte. Specifically, EIS was recorded and the serial resistance was determined from the high-frequency interception of the impedance spectrum with the real part of the complex impedance. The serial resistance is related to the conductivity of the YSZ according to equation (1), in which σ_{YSZ} is the conductivity of the YSZ electrolyte, A is the area of the cell and l is the thickness of the electrolyte. The temperature dependency of σ_{YSZ} is given in equation (2), and by combining (1) and (2) it was possible to precisely determine the temperature of the sample from the recorded EIS,

$$R_{\text{Serial}} = \frac{1}{\sigma_{YSZ}} \frac{l}{A}, \tag{1}$$

$$\sigma_{YSZ}\, S\,[\text{cm}] = 3.34 \times 10^4 \exp(-10300/T). \tag{2}$$

The heating rate for the sample was ~10 K min^{-1}. The sample was tilted approximately 45° compared with the light beam from the lamp. The gases (21% O_2 in He and pure He) were supplied through mass flow controllers, usually with a flow rate of 20–50 ml min^{-1}. Different oxygen partial pressures were obtained by mixing the gas flows appropriately.

2.3. EIS and XANES measurements

The tests were carried out at beamline A1, HASYLAB (Hamburger Synchrotronstrahlungslabor) at DESY (Deutsches Elektronen-Synchrotron) in Hamburg. A 1/2 demagnified focused beam provided a working range of 2.4–8.3 keV. Two Si 111 crystal pairs are installed as monochromators. In order to focus the beam and effectively suppress higher harmonics, two mirrors can be used, one Ni coated and one partly Ni coated and uncoated SiO_2.

The cell was positioned between the first ionization chamber (after the incoming synchrotron beam) and the second one (before the chamber for reference foils).

A passivated implanted planar silicon (PIPS) detector was used for the detection of fluorescence X-rays from the sample. The current through the PIPS detector was measured using a Keithley 428 current meter. Two Mylar foils were used to shield the light from the spectroelectrochemical cell.

The used XANES energy ranges and step sizes for the relevant metals are summarized in Table 1. XANES spectra were recorded periodically during heating and at constant temperature without and under polarization. The raw data were treated using the program *WinXAS*. Typically, the spectra were smoothed using the Fourier function. The first inflection point (zero of the second derivative) was assigned

Table 1
Energy intervals and step sizes for XANES measurements.

Fe edge: 7112 eV				
Energy (eV)	7063	7107	7140	7210
Step size (eV)	0.5	0.1	0.5	Stop
Co edge: 7709 eV				
Energy (eV)	7660	7704	7737	7807
Step size (eV)	0.5	0.1	0.5	Stop

the edge. The background was corrected using two linear functions and the edge jump was normalized to unity.

The energy calibration was established before and after the *in situ* experiments with absorption measurements on a 5 µm-thick Cr metal foil, which was placed between the second and third ionization chamber.

For impedance spectra and polarization of the cells, a Gamry Reference 600 Potentiostat was used. The impedance spectra were recorded in the frequency range 1 MHz–0.1 Hz with the voltage amplitude 36 mV r.m.s. and six points recorded per decade. The thin-film electrode/working electrode assembly of the fuel cell was polarized cathodically at −100 mV, −300 mV and −500 mV for 1–2 h.

3. Results and discussion

3.1. Selection of samples

The probing depth for the *K*-edges of the investigated transition metals using a fluorescence detector is several micrometres, depending on the intensity of the incoming beam. The recorded spectra therefore truly represent the bulk material, since the measurements in the used mode are not surface sensitive (like, for example, in total-electron-yield measurements). Thin-film electrodes were chosen for this study because a change in oxidation state owing to the polarization should be easier to detect on thin-film electrodes compared with conventional porous electrodes for the following reason: when a conventional screen-printed electrode of 20–30 µm thickness is polarized, the current flow owing to the migration of O^{2-} ions, and thereby the change in oxidation states in the electrode material, will be largest in the electrode part closest to the electrolyte (Nielsen *et al.*, 2011). As the XANES spectrum is probing the bulk, a XANES spectrum recorded on conventional electrodes under polarization will probably not be able to detect the changes in the oxidation states occurring only in the deeper electrode layers closer to the electrolyte. By choosing a thin-film sample of ∼300 nm thickness, the O^{2-} migration and change in oxidation state is expanded through the entire thin film, and will therefore be better detectable in the XANES spectrum.

3.2. XANES verification

The fuel cells contained LSCF layers that are used for SOFC cathodes on a YSZ electrolyte. In order to assign the comparability of XANES spectra of LSCF for different sample compositions, preparations, measuring conditions and XANES configurations, room-temperature XANES spectra were recorded. In Fig. 3 (for values see Table 2), room-temperature Fe XANES spectra for two fuel cells from different batches are shown together with a LSCF powder pressed to a pellet with alumina and measured previously at room temperature in the XANES cell described by Hagen (2011). The spectra show pre-edge features originating from 1*s* to 3*d* transitions, while the white line (maximum at the edge) is due to dipole-allowed 1*s* to 4*p* transitions [for a detailed discussion see also Haas *et al.* (2009)]. The edge energies for the main Fe edge were around 7.128 keV in all cases (7.1282 and 7.1283 keV for the two fuel cells). Consequently, comparing the two different types of LSCF samples, a good agreement can be concluded. The LSCF electrodes in the two fuel cells from different batches yield almost identical XANES spectra; small differences are only visible after the pre-edge feature, which indicate a robust and reproducible way of sample preparation and measurement.

Table 2
Edge energy values for LSCF in fuel cells ($La_{0.58}Sr_{0.4}Co_{0.2}Fe_{0.8}O_{3-\delta}$), measured in the spectroelectrochemical cell, LSCF powder 1 ($La_{0.3}Sr_{0.7}Co_{0.5}Fe_{0.5}O_{3-\delta}$) and LSCF powder 2 [$(La_{0.6}Sr_{0.4})_{0.99}Fe_{0.8}Co_{0.2}O_3$], both measured in the XANES cell presented by Hagen (2011), obtained from XANES spectra at room temperature and 773 K or 873 K.

	Room temperature	773 K	873 K	ΔE
Fe XANES edge				
Fuel cell (eV)	7128.2		7127.8	0.4
Powder 1 (eV)	7128.1	7128.0		0.1
Powder 2 (eV)	7127.3			
Co XANES edge				
Fuel cell (eV)	7726.0		7724.9	1.1
Powder 1 (eV)	7724.6	7723.7		0.9
Powder 2 (eV)	7724.1			

The Co valence (and thus edge) is very sensitive to the stoichiometry/oxygen vacancies of the perovskite sample. Therefore, the edge energies are to some extent different for

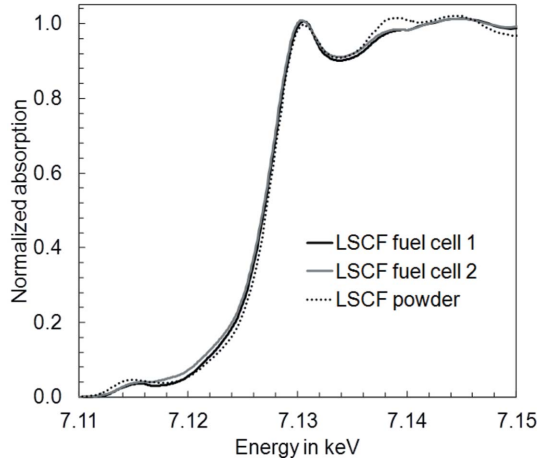

Figure 3
Room-temperature Fe XANES spectra of two fuel cells with LSCF layers deposited on YSZ from two batches (measured in 21% O_2 in He using fluorescence detector in the spectroelectrochemical cell) and one LSCF powder, pressed into a pellet using alumina [measured in air in transmission, in the *in situ* cell presented by Hagen (2011)].

the different LSCF samples (see Table 2), where the formal valence of Co at room temperature is in the order $La_{0.58}Sr_{0.4}Co_{0.2}Fe_{0.8}O_{3-\delta}$ (fuel cell) > $(La_{0.6}Sr_{0.4})_{0.99}Fe_{0.8}Co_{0.2}O_3$ (powder 2) $\simeq$ $La_{0.3}Sr_{0.7}Co_{0.5}Fe_{0.5}O_{3-\delta}$) (powder 1). Thus, the differences can be related to the chemical composition of the LSCF samples and not to the configuration of the XANES set-up.

The fuel cells were heated to 873 K in 21% O_2 in He. In Fig. 4 the Fe and Co XANES spectra are shown for room temperature and 873 K. For the case of iron, only small changes were observed comparing room temperature and 873 K spectra. Quantitative analysis revealed a change of the edge energy by 0.4 eV towards lower energies (see Table 2). Such a small change is close to the error of the measurement of 0.1–0.2 eV. Evaluating the cobalt in the LSCF, on the other hand, a significant shift of the XANES spectrum towards lower energies was observed. The energy value for the main absorption edge decreased by 1.1 eV, indicating a reduction of cobalt ions in the perovskite structure from four to lower valance. The same effect was observed when a LSCF powder was studied, although the highest temperature in this case was only 773 K and the gas atmosphere was synthetic air (see Table 2).

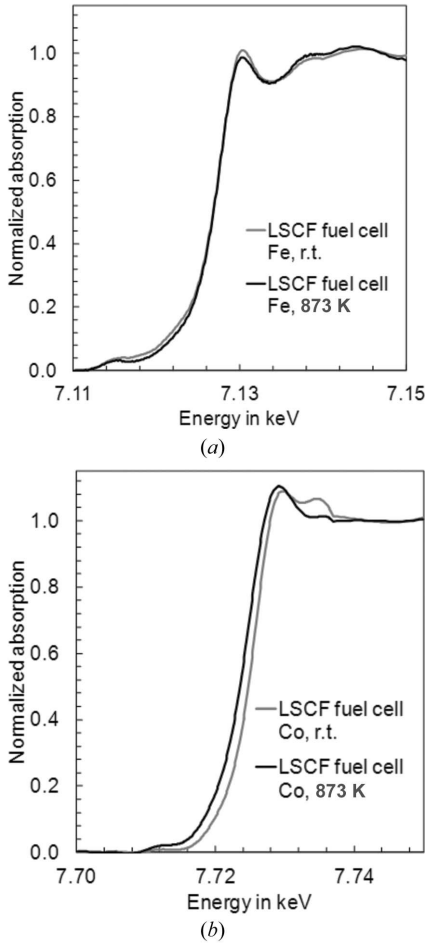

Figure 4
Fe-XANES (*a*) and Co-XANES (*b*) spectra of the fuel cell with LSCF electrodes recorded at room temperature and at 873 K in 21% O_2 in He.

The positions of the energy features (threshold, pre-edge peak, main edge and 1*s* to 4*p* transition) in XANES spectra of metal oxides are strongly dependent on the oxidation state of the absorbing transition metal. It was found that they shifted linearly to higher-energy values (so-called chemical shift) with increasing oxidation state of the metal (Wong *et al.*, 1984). In addition to the valence, the chemical shift is due to electronegativity of ligands, coordination number and other structural features. Typically, the edge energy shifts by 2–4 eV when the oxidation state shifts by one unit [see, for example, Wong *et al.* (1984) and Rasmussen *et al.* (2003) for vanadium, Figueroa *et al.* (2005) for manganese, and Le Toquin *et al.* (2006) for copper in different oxidic structures]. In the present studies the energy shift of 1.1 eV would correspond to a mean oxidation state of cobalt in the reduced state of $\sim$3.7 or a reduction of up to $\sim$1/3 Co(IV) to Co(III) ions [see also discussion in Hagen & Mikkelsen (2005)].

The partial reduction of Co ions in the LSCF perovskite structure can be related to the change of the oxygen stoichiometry in samples of the general formula $La_{1-x}Sr_xCo_{1-y}Fe_yO_{3-\delta}$, where δ expresses the degree of oxygen non-stoichiometry. It was found by, for example, temperature-programmed reduction and solid electrolyte coulometry that δ increased with increasing temperature, decreasing oxygen partial pressure and increasing Sr or Co content (Mantzavinos *et al.*, 2000; Scott *et al.*, 2002).

Using the edge energy shift obtained by XANES between room and elevated temperature in this work and the related estimated portion of reduced Co in the perovskite, a δ of $\sim$0.05 can be estimated. This value fits well into the general trend found by Scott *et al.* (2002) or by Plonczak *et al.* (2012). The strength of the XANES method as applied here is that the reduction as a consequence of a change of the oxygen stoichiometry can be mainly related to the Co ions in the perovskite. With these first measurements at room and elevated temperature, the spectroelectrochemical cell was verified with regard to choice of sample (powder *versus* fuel cell), temperature (different heating methods and temperature probes) and reproducible XANES spectra (transmission *versus* fluorescence in different set-ups).

3.3. EIS verification

The electrochemical properties were studied by EIS at temperatures around 873 K. In order to verify the spectroelectrochemical cell regarding EIS, the results are compared with impedance spectra recorded in a typical set-up for EIS on symmetric cells with thin-film LSCF electrodes on both sides of a YSZ electrolyte crystal ('thin-film cells'). In Fig. 5 the impedance spectra are presented by Nyquist and Bode plots.

The primary resistance values obtained from the Nyquist plot of impedance spectra of an electrochemical cell are the serial and the polarization resistance (see Fig. 5*a*). The serial resistance (R_s) in the impedance plot is the value of the high-frequency interception of the curve with the real part of the complex impedance and originates mainly from the ohmic

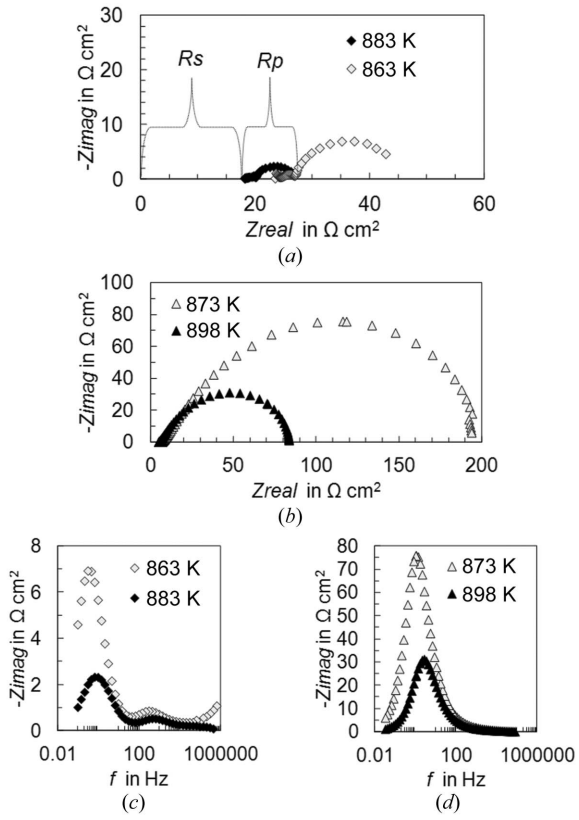

Figure 5
Impedance spectra, Nyquist plots (*a*, *b*) and Bode plots (*c*, *d*) measured on the fuel cell in the spectroelectrochemical cell at 863 K and 873 K in 21% O_2 in He (*a*, *c*), and on the thin-film cell, measured in the EIS set-up at 873 K and 898 K in 100% O_2 (*b*, *d*). R_s and R_p are illustrated on the impedance spectrum at 883 K (*a*).

resistance of the electrolyte. This value is for a given electrolyte (and known thickness) correlated with the temperature [see equations (1) and (2)]. The polarization resistance (R_p) is the difference between the low- and high-frequency interceptions (see Fig. 5*a*) and is a measure of the losses (activity) of the electrode. The smaller the resistance, the more active is the electrode. Further, time-resolved elementary processes on the electrode appear as single arcs that partly overlap in the polarization part of the plot. They become more visible in a first approximation by the Bode plot of the impedance spectrum [see Figs. 5(*c*) and 5(*d*)]. The impedance spectra are sensitive to the structural and compositional characteristics of a specific electrode, and the operating conditions.

The impedance spectrum of the fuel cell (Fig. 5*a*) yields the combined resistances from both electrodes, one being a thin-film LSCF electrode and the other a porous LSCF/CGO composite. By far the largest impedance contribution [factor ~100, compare with typical values for porous LSCF-based cathodes in Nielsen *et al.* (2011)] arises from the thin-film electrode, owing to the small surface area and thus very low activity. When evaluating the impedance spectra, the focus can therefore be placed on the thin-film electrode.

The two impedance spectra in Fig. 5(*a*) were obtained at 863 and 883 K. The increase of the temperature by only 20 K leads to a decrease of the polarization (electrode) resistance by a factor of ~3, which corresponds to an increase of the electrochemical activity. In Fig. 5(*b*) the impedance spectra of the thin-film cells measured in the EIS set-up are shown for two temperatures. A significantly larger polarization resistance was obtained at 873 K (the same temperatures as in the spectroelectrochemical cell). This could be due to a thicker electrode and/or lower surface area. By increasing the temperature to 898 K, the polarization resistance decreased significantly and thus the trend measured in the spectroelectrochemical cell was confirmed.

The Bode plots for both cells [Fig. 5(*c*) and 5(*d*)] indicate a pronounced process around frequencies of 1 Hz, which is assigned to oxygen stoichiometry changes in the LSCF thin-film electrodes.

Despite the different absolute values for the polarization resistances, the spectra obtained in the spectroelectrochemical cell and the EIS set-up show, in general, similar characteristics and trends with temperature and the results from the first can be used to evaluate electrochemical properties simultaneously with XANES.

3.4. Polarization of the fuel cell

As outlined in the *Introduction*, the ultimate objective is to characterize electrochemical cells under operating conditions that include the effect of polarization. The fuel cell was heated to 873 K and subjected to different potentials. Impedance spectra were recorded and XANES spectra as well. Polarization changes the local pO_2 and is thus expected to affect the oxidation state of cobalt in particular (Orikasa *et al.*, 2011).

During the heating, the periods of polarization and the periods at open circuit voltage, Co and Fe XANES spectra were recorded. In Fig. 6 the edge energy values for Co and Fe, the polarization and temperatures are shown over the whole

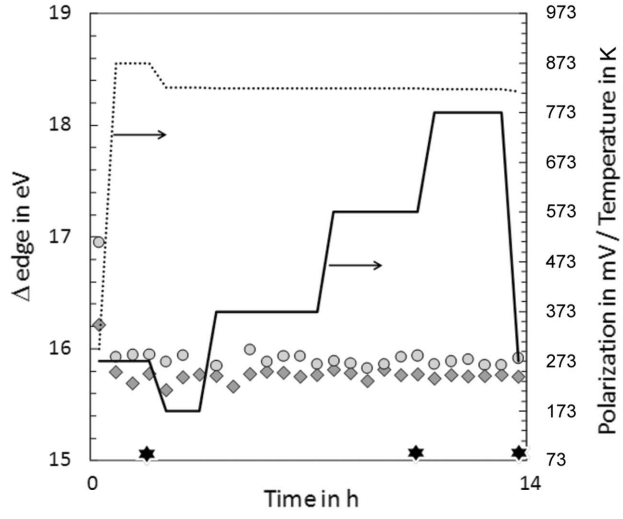

Figure 6
Co (circles) and Fe (diamonds) edge energies deduced from XANES spectra, expressed as ΔE ($E_{edge} - E_{edge\text{-}Me}$), are shown for the whole test sequence together with the polarization (full line) and temperature (dotted line); the stars on the time axis mark the times of recording impedance spectra (shown in Fig. 7).

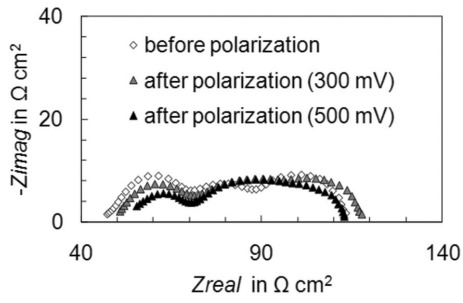

Figure 7
Impedance spectra of the fuel cell with LSCF electrodes recorded in 21% O_2 in He in the spectroelectrochemical cell before polarization (open symbols, 873 K), after polarization at initially −100 mV, later 100 mV, followed by 300 mV (grey symbols, 823 K), and after additional ∼3 h polarization at 500 mV (black symbols, 823 K).

test sequence. When heating from room temperature to 873 K without polarization, the edge energies for Co and Fe decreased, more significantly for cobalt (see Table 2), indicating a reduction of mainly cobalt ions in the perovskite structure, as presented and discussed in §3.2. In the period following the start of polarization at different degrees, both edge energies remained almost constant. The XANES spectra demonstrated that temperature has a larger effect on the oxidation states of cobalt (and iron) than polarization.

In Fig. 7 impedance spectra recorded before and after polarization at 300 and 500 mV are shown. Only small changes have occurred. The slight change of the serial resistance is most likely due to small temperature changes and not a result of the polarization. The spectrum recorded after exposure to the highest polarization of 500 mV indicates a slight decrease of the polarization resistance, *i.e.* the electrode seems to have activated. In general, the EIS results from before and after polarization are thus in line with the obtained XANES spectra, where no significant changes were observed as an effect of the polarization (see Fig. 6). It can be argued whether there should have occurred more significant changes of the oxidations states of cobalt and iron owing to polarization. The following issues have to be considered. The magnitude of polarization could be an important factor, *i.e.* that it was too low in this study to induce changes. Electrode thickness could be another parameter, even though the measurements were made on thin-film electrodes in this study. Further, the oxygen non-stoichiometry of the thin-film electrode used in this study could be a reason why no significant effects were observed owing to polarization. It has been shown to be lower when compared with bulk samples, maybe owing to 'imperfect' thin films (Plonczak *et al.*, 2012). The lower oxygen-nonstoichiometry means a lower number of positive ions with a change in polarization state during polarization and thus a smaller effect observable by XANES.

Future work should comprise thin layers of porous LSCF electrodes with a larger oxygen non-stoichiometry and cathodes with varying Co/Fe ratios to explore the mechanism of oxygen reduction under polarization in the SOFC in more detail.

4. Conclusion

The spectroelectrochemical cell used in this study for the first time proved to be able to provide reliable data for electrical impedance and for XANES under relevant conditions of a fuel cell, *i.e.* at elevated temperature, in the presence of relevant gases and under polarization. It has the potential to measure on a real solid oxide fuel cell and thus provide simultaneously information about the electrochemical performance and state of the transition metal components in the electrodes under operation.

Fuel cells with thin-film LSCF electrodes were studied at ∼873 K in synthetic air. When heating from room temperature, cobalt ions in the perovskite structure were reduced. The application of a polarization on the electrodes did not affect the oxidation states of iron or cobalt. Neither were the electrochemical properties, *i.e.* electrode processes, affected to a large extent as revealed by electrical impedance spectroscopy.

Further investigations are needed to reveal the effects of polarization, electrode composition and structure, pO_2, *etc.* on the electrode activity and the related characteristic oxidation states of the electrode components. Furthermore, a refined study might be able to distinguish processes occurring at the electrode/electrolyte interface from bulk processes in the electrode.

HASYLAB is gratefully acknowledged for providing beamline facilities and technical support. The authors thank Pawel Plonczak for providing EIS of thin film samples for comparison and for manufacturing the thin-film electrodes studied in this work, and Martin Soegaard for fruitful scientific discussions. This work was supported by The Programme Commission on Sustainable Energy and Environment, The Danish Council for Strategic Research, *via* the Strategic Electrochemistry Research Center (SERC) (http://www.serc.dk/), contract No. 2104-06-0011.

References

Backhaus-Ricoult, M., Adib, K., St Clair, T., Luerssen, B., Gregoratti, L. & Barinov, A. (2008). *Solid State Ion.* **179**, 891–895.
Braun, A., Shrout, S., Fowlks, A. C., Osaisai, B. A., Seifert, S., Granlund, E. & Cairns, E. J. (2003). *J. Synchrotron Rad.* **10**, 320–325.
Figueroa, S. J. A., Requejo, F. G., Lede, E. J., Lamaita, L., Andres Peluso, M. & Sambeth, J. E. (2005). *Catal. Today*, **107–108**, 849–855.
Haas, O., Vogt, U. F., Soltmann, C., Braun, A., Yoon, W.-S., Yang, X. Q. & Graule, T. (2009). *Mater. Res. Bull.* **44**, 1397–1404.
Hagen, A. (2011). *Chem. Phys. Lett.* **502**, 235–240.
Hagen, A. & Mikkelsen, L. (2005). *Proceedings of the 26th Risø International Symposium on Materials Science: Solid State Electrochemistry*, edited by S. Linderoth, A. Smith, N. Bonanos, A. Hagen, L. Mikkelsen, K. Kammer, D. Lybye, P. V. Hendriksen, F. W. Poulsen, M. Mogensen and W. G. Wang, pp. 197–202, Risø National Laboratory, Roskilde, Denmark.
Højgaard Jensen, S., Hjelm, J., Hagen, A. & Mogensen, M. B. (2009). *Handbook of Fuel Cells*, p. 1090. New York: Wiley.
Huang, K. & Goodenough, J. B. (2009). Editors. *Solid Oxide Fuel Cell Technology: Principles, Performance and Operations.* Oxford: Woodhead.

Knibbe, R., Hauch, A., Hjelm, J., Ebbesen, S. D. & Mogensen, M. (2011). *Green*, **1**, 141–169.
Le Toquin, R., Paulus, W., Cousson, A., Prestipino, C. & Lamberti, C. (2006). *J. Am. Chem. Soc.* **128**, 13161–13174.
Lu, X., Faguy, P. W. & Liu, M. (2002). *J. Electrochem. Soc.* **149**, A1293–A1298.
Mantzavinos, D., Hartley, A., Metcalfe, I. S. & Sahibzada, M. (2000). *Solid State Ion.* **134**, 103–109.
Mueller, N., De Souza, R. A., Brendt, J., Samuelis, D. & Martin, M. (2009). *J. Mater. Chem.* **19**, 1960–1963.
Nielsen, J., Jacobsen, T. & Wandel, M. (2011). *Electrochem. Acta*, **56**, 7963–7974.
Orikasa, Y., Ina, T., Nakao, T., Mineshige, A., Amezawa, K., Oishi, M., Arai, H., Ogumi, Z. & Uchimoto, Y. (2011). *Phys. Chem. Chem. Phys.* **13**, 16637–16643.
Plonczak, P., Bierberle-Hütter, A., Søgård, M., Hendriksen, P. V. & Gauckler, L. J. (2012). *J. Electrochem. Soc.* **159**, B1–B12.
Pomfret, M. B., Owrutsky, J. C. & Walker, R. (2010). *Annu. Rev. Anal. Chem.* **3**, 151–174.
Rasmussen, S. B., Hagen, S., Masters, S., Hagen, A., Ståhl, K., Eriksen, K. M., Simonsen, P., Jensen, J. N., Berg, M., Chorkendorff, I. & Fehrmann, R. (2003). *PowerPlant Chem.* **5**, 360–369.
Rodriguez, M. A., Ingersoll, D. & Doughty, D. H. (2000). *Adv. X-ray Anal.* **42**, 267–275.
Scott, S. P., Mantzavinos, D., Hartley, A., Sahibzada, M. & Metcalfe, I. S. (2002). *Solid State Ion.* **152–153**, 777–781.
Simonsen, V. L. E., Nørskov, L., Hagen, A. & Kammer Hansen, K. (2009). *J. Solid State Electrochem.* **13**, 1529–1534.
Wong, J., Lytle, F. W., Messmer, R. P. & Maylotte, D. H. (1984). *Phys. Rev. B*, **30**, 5596–5610.
Yildiz, B., Chang, K.-C., Myers, D., Carter, J. D. & You, H. (2006). *Proceedings of the 7th European Solid Oxide Fuel Cell Forum*, 3–7 July 2006.